LASER INTERFEROMETER GRAVITATIONAL WAVE OBSERVATORY
--LIGO—
California Institute of Technology
Massachusetts Institute of Technology

Document Number: **LIGO- T020143-00-R** Date: 09/28/02

Author: Aya Sekido

Measurement of the laser beam profile at the 40 Meter Prototype Interferometer

This is an internal working note
of the LIGO Laboratory.

California Institute of Technology
LIGO Laboratory, MS 18-34
1200 E. California Blvd.
Pasadena, CA 91125
Phone (626) 395-3064
Fax (626) 304-9834

Massachusetts Institute of Technology
LIGO Laboratory, NW17-161
175 Albany St.
Cambridge, MA 01239
Phone (617) 253-4824
Fax (617) 253-7014

LIGO Hanford Observatory
P.O. Box 159
Richland, WA 99352
Phone (509) 372-8106
Fax (509) 372-8137

LIGO Livingston Observatory
P.O. Box 940
Livingston, LA 70754
Phone (225) 686-3100
Fax (225) 686-7189

Measurement of the laser beam profile at the 40 Meter Prototype Interferometer

Aya Sekido
Waseda University
Mentors: Alan Weinstein, Osamu Miyakawa
LIGO SURF Program, 2002

Abstract

The Caltech 40 Meter interferometer is being upgraded to prototype the Advanced LIGO optical configuration and controls. The interferometer requires an infrared laser beam of extremely high stability in frequency, intensity, launch position and angle, and transverse profile – the Pre-Stabilized Laser (PSL). In this report, we present the results of studies of the transverse profile and stability of the beam at the point where it leaves the PSL table and enters into the vacuum system. We discuss the tuning of the mode matching from the PSL to the input mode cleaner optical cavity, and the position and launch angle stability of the beam.

Table of Contents

1 Introduction

The detection of gravitational waves is a true 20th century scientific adventure. Albert Einstein predicted the existence of gravitational waves in 1916. Russell Hulse and Joseph Taylor proved the existence of gravitational waves indirectly by observing the rate of inspiral of the binary pulsar PSR1913+16 in 1974. However, as of now no one has detected gravitational waves directly. As radio astronomy discovered the cosmic microwave background (1965), pulsars (1967), and many other things, we hope that gravitational wave astronomy will discover new and interesting objects some day. Various detectors have been developed to detect gravitational waves directly, including the Laser Interferometer Gravitational-Wave Observatory (LIGO) in the US and TAMA in Japan. These detectors aim to detect gravitational waves in the next few years.

The initial LIGO detectors at Hanford, Washington and Livingston, Louisiana are currently taking their first scientific observations. Because the observation of gravitational waves with these detectors is not assured, plans are in progress for upgrading them to an Advanced LIGO configuration, including a more complex optical configuration known as dual recycling. The optical configuration and controls for an Advanced LIGO interferometer is being prototyped at the Caltech 40 Meter interferometer laboratory.

The interferometer being developed at the 40 Meter lab requires an infrared laser beam of extremely high stability in frequency, intensity, launch position and angle, and transverse profile. This beam is currently supplied by an Initial-LIGO-like pre-stabilized laser (PSL). The block diagram of this laser system is shown in Figure 1.

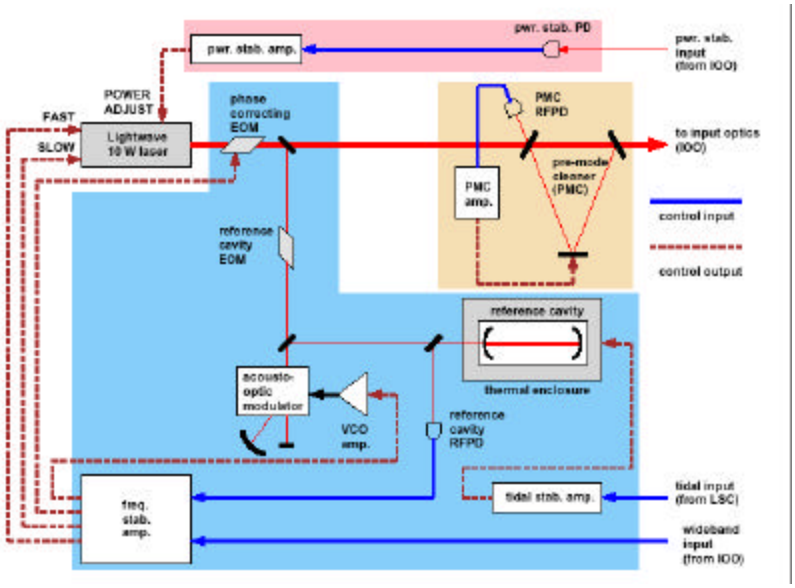

Figure 1: Block diagram of the LIGO Pre-Stabilized Laser (PSL).

The active components of the PSL include:

- A Lightwave 10-watt Nd^{3+}:YAG laser emitting infrared radiation at a wavelength of 1.064 μm.
- A Frequency Stabilization servo loop, including a frequency reference cavity and associated sensing and actuation.
- A Pre-Mode-Cleaner (PMC) triangular optical cavity and associated servo sensing, actuation, and electronics. The eigenmode resonating in the PMC serves to define the beam's transverse profile downstream of it.
- A non-yet-installed intensity stabilization servo.

All of these components reside on a single optical table, shown in Figure 2, surrounded by a laser safety enclosure. Also sharing that table are the following components of the Input Optics:

- A pair of mode matching lenses to refocus the beam from the PMC to the EOMs.
- Three electro-optic modulators (EOMs, also known as pockels cells or optical phase modulators) which apply RF sidebands to the beam at 29.48 MHz, 33.21 MHz, and 166.0 MHz, in order to sense deviations from resonance of the downstream optical cavities via Pound-Drever-Hall locking. (Only the first two of these EOMs were installed at the time of this work). Because the EOM aperture is rather small (2 mm for the New Focus Model 4003), the beam is required to have a waist in the second EOM.
- A second pair of mode matching lenses to refocus the beam from the EOMs to the 13 meter suspended mass mode cleaner inside the vacuum system. The mode cleaner was being commissioned during the time of this work.
- A pair of PZT-actuated steering mirrors, used to steer the beam into the mode cleaner.
- A periscope to raise the beam to the appropriate height for insertion into the vacuum chambers containing the mode cleaner and the main interferometer.
- An Input Optics diagnostic optical train (shown in Figure 3), viewing a portion of the beam picked off at the periscope just before insertion into the vacuum chambers. This optical train contained a power monitoring photodiode, two quadrant photodiodes with associated optics to monitor beam position and angle, a digital camera, and an optical spectrum analyzer.

1.1 Purpose of this work

The main goals of this work are to

- Measure the laser beam profile in the Input Optics part of the beam path, and determine the best positions of the mode matching lenses that optimally match the beam transverse profile from the PMC to the EOMs, and from the EOMs to the suspended mass mode cleaner ~ 6 meters away.
- Commission and calibrate the two quadrant photodiodes that monitor beam position and angle, and measure the beam position and angle fluctuations.

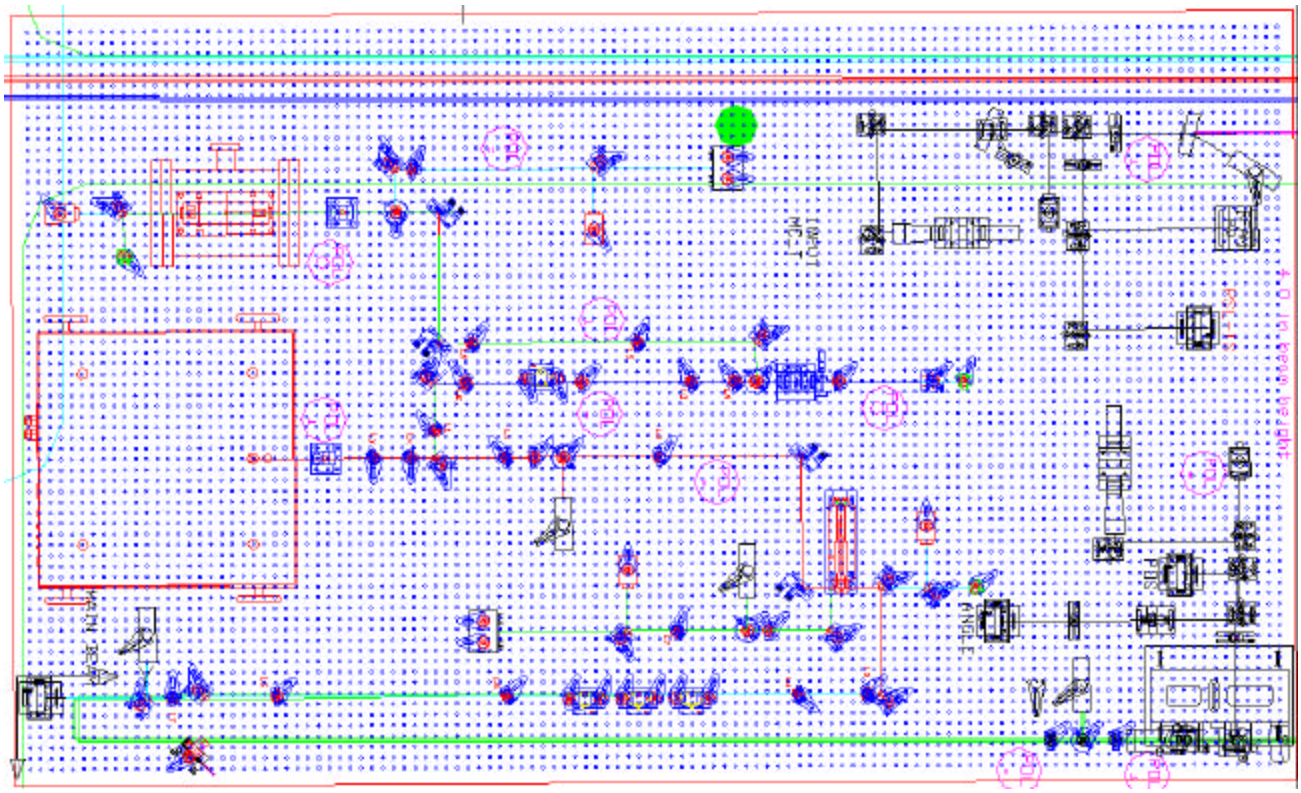

Figure 2: Layout of the PSL optical table at the 40 Meter laboratory. The Lightwave laser is in the left center. The three EOMs are in the center bottom. The periscope and input optics monitoring is in the lower right.

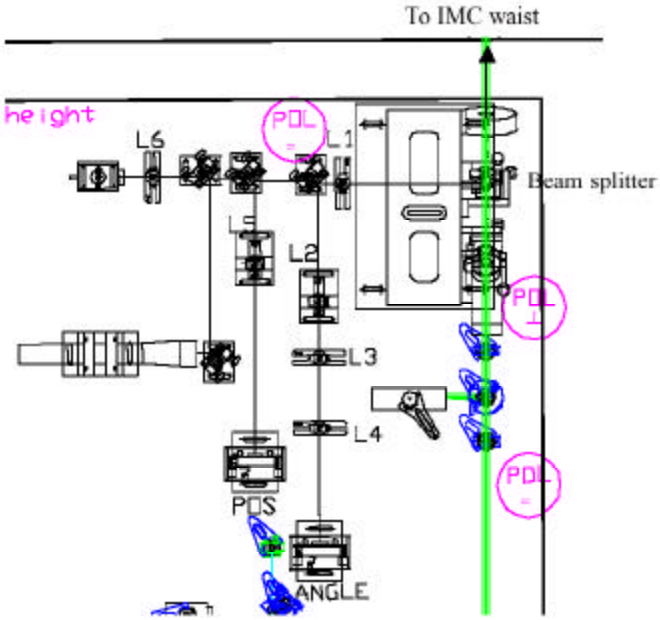

Figure 3: The input optics monitoring system.

2 Gaussian Beams

The equations of Gaussian beams are very widely used in analyzing laser beams. Here, we use this knowledge to adjust the mode-matching lenses. In this chapter we derive the Gaussian beam equations, and introduce two important parameters, which are the beam waist and curvature.

2.1 Paraxial wave equation

The paraxial wave equation is a fundamental equation in the derivation of the Gaussian beams equations, given from Maxwell's equations with the *paraxial approximation*.

Electromagnetic fields are governed by the scalar wave equation.

$$(\nabla^2 + k^2)\cdot \vec{E}(x,y,z) = 0 \qquad (1)$$

We assume that the phase profile of laser beams changes with distance along z axis, which is the beam propagation direction. We can write the electromagnetic fields in the following form.

$$\vec{E}(x,y,z) \equiv \vec{y}(x,y,z)\exp(-ikz) \qquad (2)$$

$\vec{y}(x,y,z)$ describes the transverse profile of the beam. We substitute this equation (2) to the equation (1).

$$\frac{\partial^2 \vec{y}}{\partial^2 x} + \frac{\partial^2 \vec{y}}{\partial^2 y} + \frac{\partial^2 \vec{y}}{\partial^2 z} - 2ik\frac{\partial \vec{y}}{\partial z} = 0 \qquad (3)$$

Then we use the *paraxial approximation*.

$$\left|\frac{\partial^2 \vec{y}}{\partial^2 z}\right| << \left|2k\frac{\partial \vec{y}}{\partial z}\right| \quad or \quad \left|\frac{\partial^2 \vec{y}}{\partial^2 x}\right| \quad or \quad \left|\frac{\partial^2 \vec{y}}{\partial^2 y}\right| \qquad (4)$$

This shows that the z dependence of $\vec{y}$ (x, y, z) will in general be slow compared to the other transverse dependence. Using this approximation we can get the *paraxial wave equation*.

$$\frac{\partial^2 \vec{y}}{\partial^2 x} + \frac{\partial^2 \vec{y}}{\partial^2 y} - 2ik\frac{\partial \vec{y}}{\partial z} = 0 \qquad (5)$$

2.2 Paraxial Spherical wave

It is convenient to presume the Paraxial Spherical wave as one of the solutions of the *paraxial wave* equation, not to solve is directly. First we derive it using paraxial assumption. After that we make sure that this *paraxial spherical* wave satisfies the paraxial wave equation.

We think about a basic spherical wave.
The images of this are shown in Figure 4.
The wave propagates from r_o, and observational point is r. The electromagnetic fields is defined as following.

$$\vec{E}(r, r_o) = \frac{\exp\left[-ikr(r, r_o)\right]}{r(r, r_o)} \qquad (6)$$

The distance from r_o to r is $r(r, r_o)$

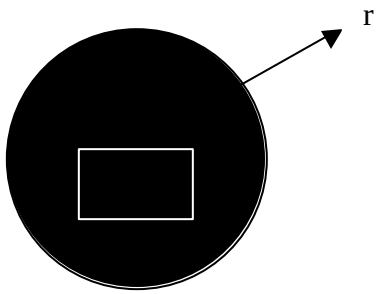

Figure4:Images of spherical wave propagation.

$$\begin{aligned} r(r, r_o) &\equiv \sqrt{(x-x_o)^2 + (y-y_o)^2 + (z-z_o)^2} \\ &= (z-z_o)\left\{1 + \frac{(x-x_o)^2 + (y-y_o)^2}{(z-z_o)^2}\right\} \\ &\cong (z-z_o) + \frac{(x-x_o)^2 + (y-y_o)^2}{2(z-z_o)} \end{aligned} \qquad (7)$$

When we induce the last equation of (7), we use this assumption; $\frac{(x-x_o)^2 + (y-y_o)^2}{(z-z_o)^2} << 1$
This means that the laser beam is located somewhere not too far off of the z axis . Then we substitute equation (7) to equation (6). Now we can get the *Paraxial Spherical wave equation*.

$$\dot{E}(r, r_o) = \frac{1}{(z-z_o)} \exp\left\{-ik(z-z_o) - ik\frac{(x-x_o)^2 + (y-y_o)^2}{2(z-z_o)}\right\} \qquad (8)$$

We recall $\vec{E}(x, y, z) \equiv \vec{y}(x, y, z)\exp(-ikz)$, and change the starting point of the wave from r_o to R_o.

$$R(z) = R_o + z - z_o \qquad (9)$$

In this equation if we substitute z_o, $R(z)$ is not zero. So we can express the wave whose source is not the origin

$$\vec{y}(x, y, z) = \frac{1}{R(z)} \exp\left\{-ik\frac{(x-x_o)^2 + (y-y_o)^2}{2(z-z_o)}\right\} \qquad (10)$$

From substituting equation (10) into (5) we easily find this equation satisfies the *paraxial wave equation*. So this equation is one of the solutions of *paraxial wave equation*.

2.3 Introducing Complex Source Point Coordinate

In the previous section we deduced one of the solutions of the paraxial wave equation, but it is not yet useful to express the actual beam. For this reason we change expediently the expression of the source of the light from real numbers to imaginary ones. It is a technical method but it gives us the convenient expression of the equation (10).

We recall the equation (10)

$$y(x,y,z) = \frac{1}{R(z)} \exp\left\{ -ik \frac{(x-x_o)^2 + (y-y_o)^2}{2(z-z_o)} \right\} \qquad (10)$$

This equation has only the phase information. However, it does not change the amplitude with distance along vertical and horizontal axes, and does not describe a real beam. The source point is altered to complex coordinate to make this equation more useful:

$$\begin{aligned} R(z) \in \Re \qquad &\longrightarrow \qquad q(z) \in \Im \\ R(z) = R_o + z - z_o \longrightarrow \qquad &q(z) = q_o + z - z_o \end{aligned} \qquad (11)$$

We divide the equation (11) between real part and imaginary part.

$$\frac{1}{q(z)} \equiv \frac{1}{q_r(z)} - i \frac{1}{q_i(z)} \qquad (12)$$

The equation (12) is substituted into the equation (10).

$$y(x,y,z) = \frac{1}{q(z)} \exp\left\{ -ik \frac{x^2 + y^2}{q_r(z)} - k \frac{x^2 + y^2}{qi(z)} \right\} \qquad (13)$$

k can be expressed in terms of the wave length: $k = 2p / l$. We define $q(z)$ again as follows:

$$\frac{1}{q(z)} \equiv \frac{1}{R(z)} - i \frac{l}{pw^2(z)} \qquad (14)$$

Here the definition of $R(z)$ has changed; it is not the equation (10). Finally we get the following equation, and this is the fundamental Gaussian beam equation.

$$\vec{y}(x,y,z) = \frac{1}{q(z)} \exp\left\{ -ik \frac{x^2 + y^2}{R(z)} - \frac{x^2 + y^2}{w^2(z)} \right\} \qquad (15)$$

In this equation not only the phase information but also the amplitude are changed with distance along vertical and horizontal axes. $R(z)$ is the radius of curvature of beams, and $w(z)$ is the beam waist: the beam has a Gaussian profile, which falls off in amplitude to 1/e of its peak amplitude ($1/e^2$ in intensity) when viewed at a distance $w(z)$ away from the beam axis ($x = y = 0$). So we can define any Gaussian laser beam if we know $R(z)$ and $w(z)$ as a function of z along the beam axis. Therefore, $R(z)$ and $w(z)$ are the most important parameters for characterizing laser beams.

In all the above, we are assuming that the laser beam is monochromatic, diffraction-limited, and has a Gaussian (TEM00) transverse profile.

3 Laser beam profile at Input Optics

3.1 Experimental apparatus

In preparation for the measurement of beam transverse profile, we investigate the properties and reliability of the BeamScan Analyzer of Photon, Inc which has a slit and a photo detector profile. The BeamScan camera and its operating principle is illustrated in Figure 4. A typical measurement of the beam transverse profile taken with the BeamScan camera and software is shown in Figure 5 and Figure 6.

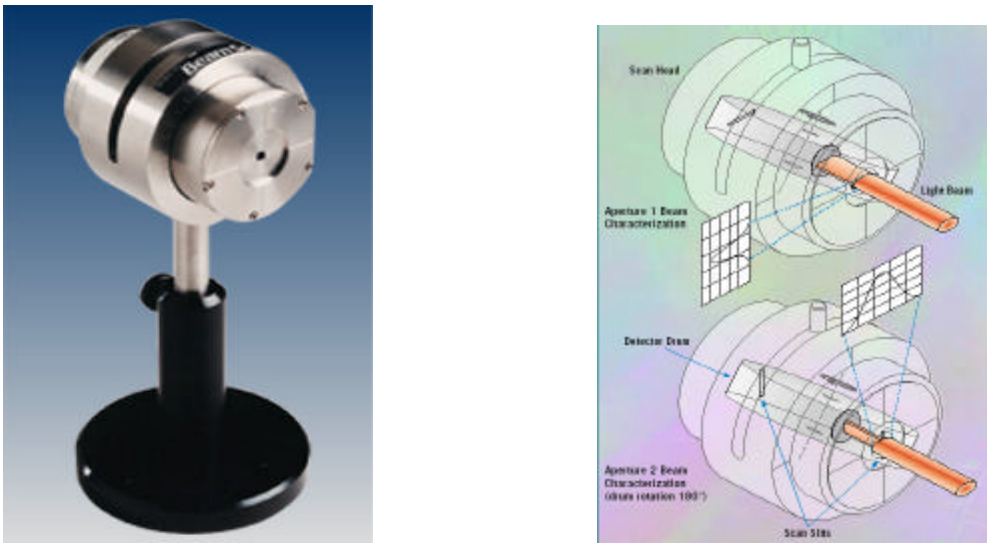

Figure 4: Left: BeamScan camera. Right: Diagram of the BeamScan head.

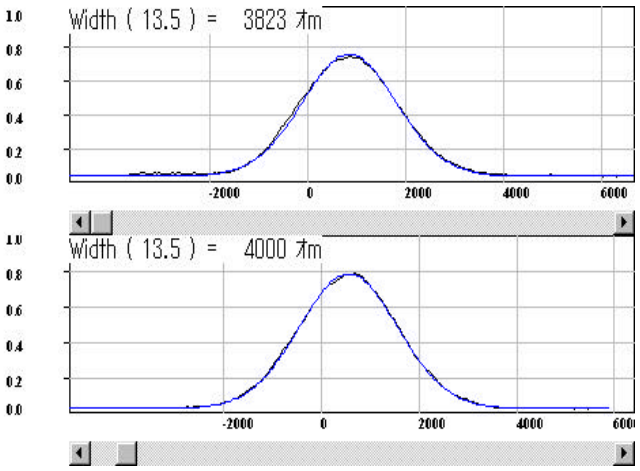

Figure 5: Results of a typical measurement of the transverse profile of the beam by the BeamScan, with the Gaussian fit and Gaussian width overlayed. Upper: horizontal beam shape; lower: vertical beam shape.

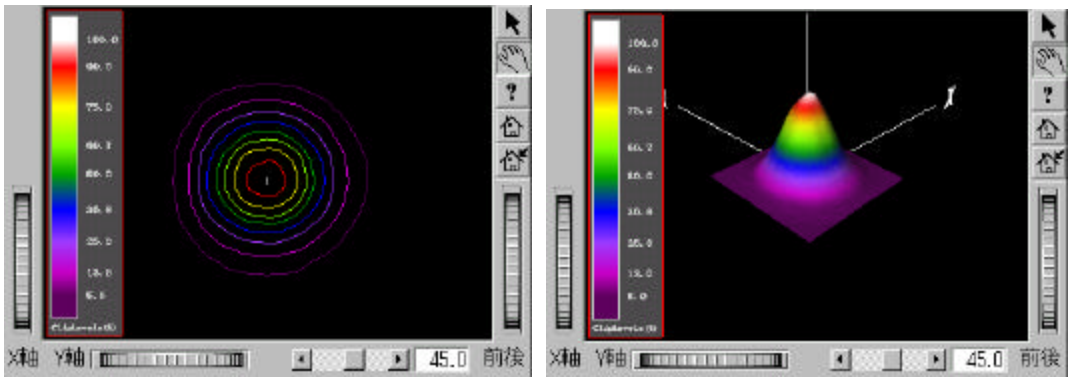

Figure 6: Two-dimensional and 3-D views of the beam transverse profile obtained using BeamScan software.

3.2 Requirements for measurement precision

The original design of transverse profile Gaussian width is shown in Figure 7. This figure shows the design value of the beam width *w(z)* as a function of distance from the laser *z*, as the beam passes through various optical components. The vertical dashed lines show the positions of the PMC and EOMs, where we desire the beam waist (minimum beam width) to occur. The vertical green lines show the locations of lenses whose purpose is to modify the transverse profile of the beam so as to place the beam waists in their desired location (mode-matching). The actual beam width should closely match this original design.

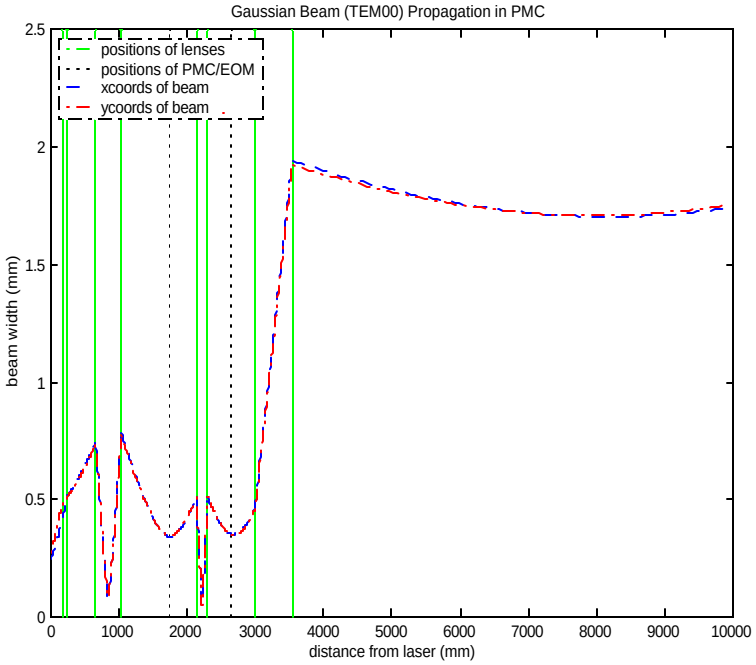

Figure 7: Beam width as a function of distance along path. Horizontal axis is distance from the laser. Vertical axis is the radius of beam width. Green vertical lines are the position of the mode matching lenses. Red and blue curves are of vertical and horizontal Gaussian beam.

Figure 7 suggests that, the required accuracy of the BeamScan for the beam width is

about ± 10 μ m.

We have two experiments to decide the accuracy of the BeamScan.

- Determine the best beam profile averaging
- Measure the power dependence

3.3 Determine the optimal beam profile averaging

The error of only 1 time measurement is too large to measure the beam width exactly. We increase the averaged number from 1 time to 100times.

3.3.1 Result: measurement of the averaging function

We obtain the following data.

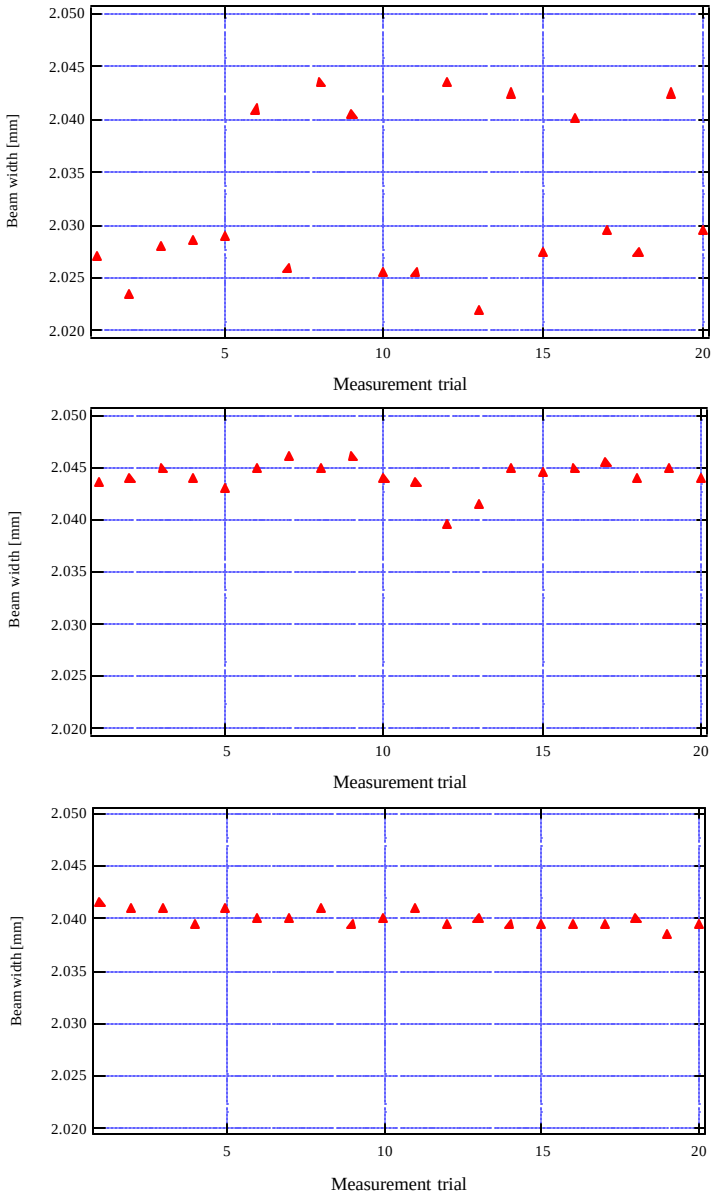

Figure 8: Repeated beam width measurements. Top: averaging 1 scan. Mi ddle: averaging 10 scans. Bottom: averaging 100 scans.

When the beam width is measured without averaging, the error of beam width is about ±0.01mm. To make the error smaller the averaging time is increased. The error in the width falls like 1/sqrt(N), where N is the number of measurements in the average.

For example the error of 10 times averaging is about ±0.03mm, and the error of 100 times averaging is about 0.002mm Finally, we conclude that the BeamScan Analyzer has enough accuracy to measure the beam width to the required precision.

3.4 The power dependence of BeamScan

3.4.1 Setup of experiment

The measurement of the beam width can depend on the laser power. We measured the power dependence using glan laser prism and half wave plate. The experimental setup for this measurement is shown in Figure 9.

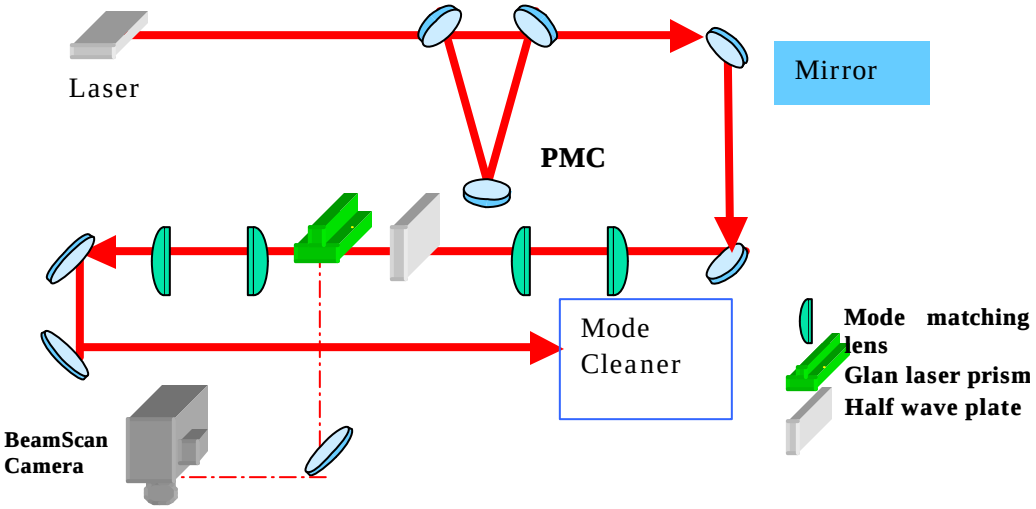

Figure 9: Set up of the experiment to measure the dependence of the beam width measurement on the beam power. A halfwave plate and a glan laser prism are placed to change the laser power of the picked off beam.

3.4.2 Result: measurement of the power dependence

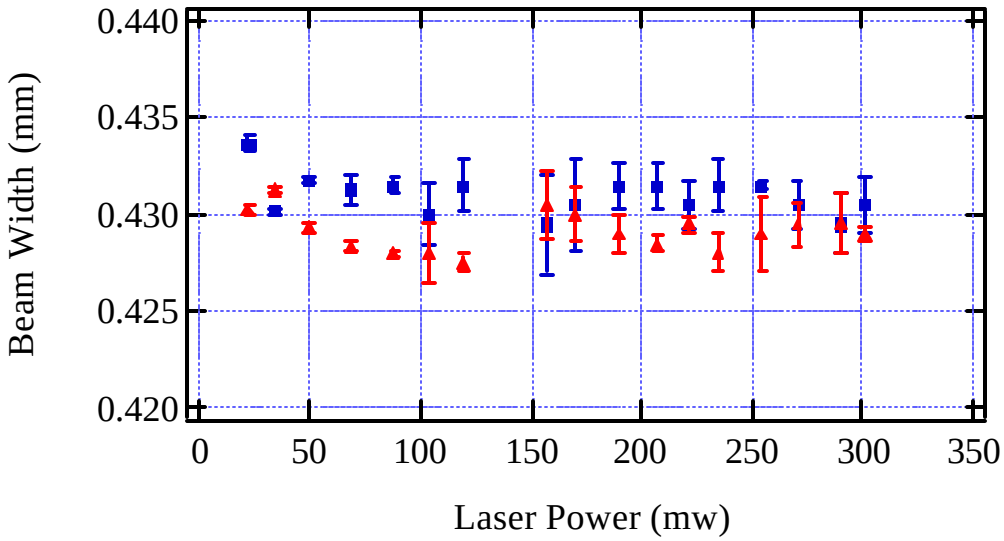

Figure 10: The beam width dependence on the laser power. Each of the blue and red makers is vertical and horizontal beam width.

Figure 10 shows the beam width dependence on the laser power. The beam width is stable between 50mw to 300mw. The error of beam width is only $\pm$5μm, which is sufficient compared with required accuracy of 10 μm.

4 Mode matching for the mode cleaner

In this experiment we measure the best positions of mode matching lenses that meets the design beam width shown in Figure 7, using the BeamScan. The transmitted light of the mode cleaner should be maximized when these lenses are placed correctly. For this purpose we take the following three steps:

- Measurement of the beam profile before adjusting the lenses
- Adjusting mode matching lenses
- Measurement of the after profile after adjusting the lenses

4.1 Measurement of the beam profile before adjusting

4.1.1 Setup for the beam profile

The mode matching lenses we used are L1, L2, L3, and L4. L1 and L2 are to be adjusted to produce a waist at the EOMs. Then, lenses L3 and L4 are to be adjusted to produce a waist at the input mode cleaner optical cavity waist. For the measurement of beam profile we set a pick off mirror to make the laser beam bend into the camera of BeamScan.

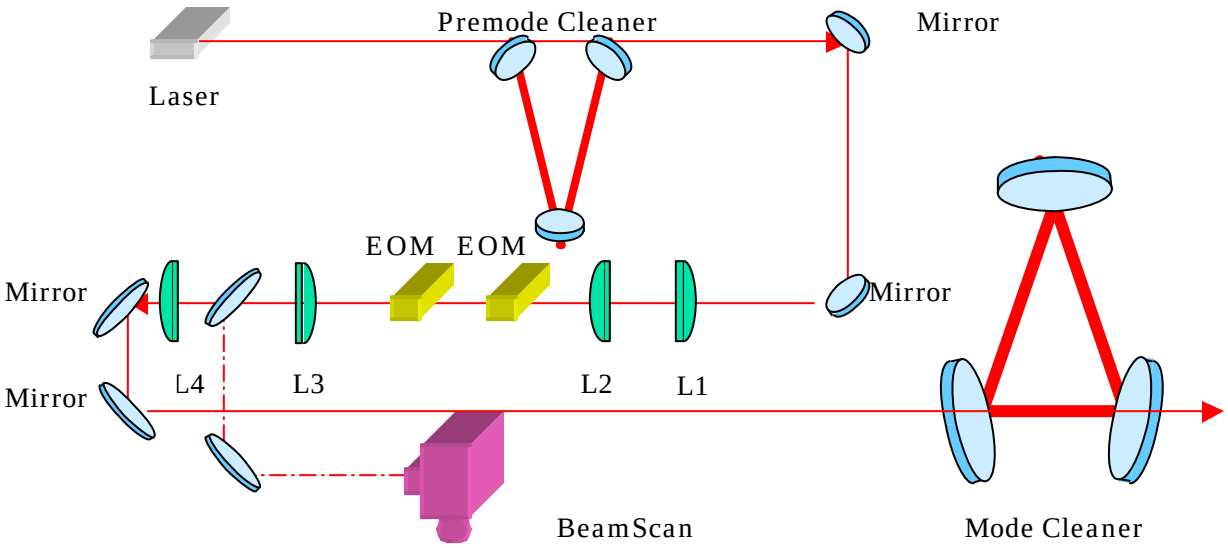

Figure 11: Set up for measurement of the beam profile. Lenses L1 and L2 are to be adjusted to produce a waist at the EOMs. Then, lenses L3 and L4 are to be adjusted to produce a waist at the input mode cleaner optical cavity waist.

The detailed location of the mode matching lenses are shown in Table 1.

Table 1: Distance of mode matching lens before adjusting.

From PSL to L1(mm)	From L1 to L2(mm)	From L2 to L3(mm)	From L3 to L4(mm)	From L4 to MC(mm)
377.0	1116.0	165.7	710	546.0

4.1.2 Result of Measurement of the beam profile before adjusting

The result of the measurement before the adjustment is shown in Figure 12.
The green lines are positions of mode matching lenses, and the red and blue makers are data we took, when some of the lenses are removed. The leftmost set of data points express the beam profile after L1 (bypassing L2). The second set is after L2. The third set is around EOM waist. The fourth set is after L3 (bypassing L4), and last set shows the waist size at a distance corresponding to the mode cleaner. The vertical dotted lines show the position of the pre-mode cleaner and EOM. After taking the following data, we calculate the waist size of the beams. These results are shown in the Table 2.

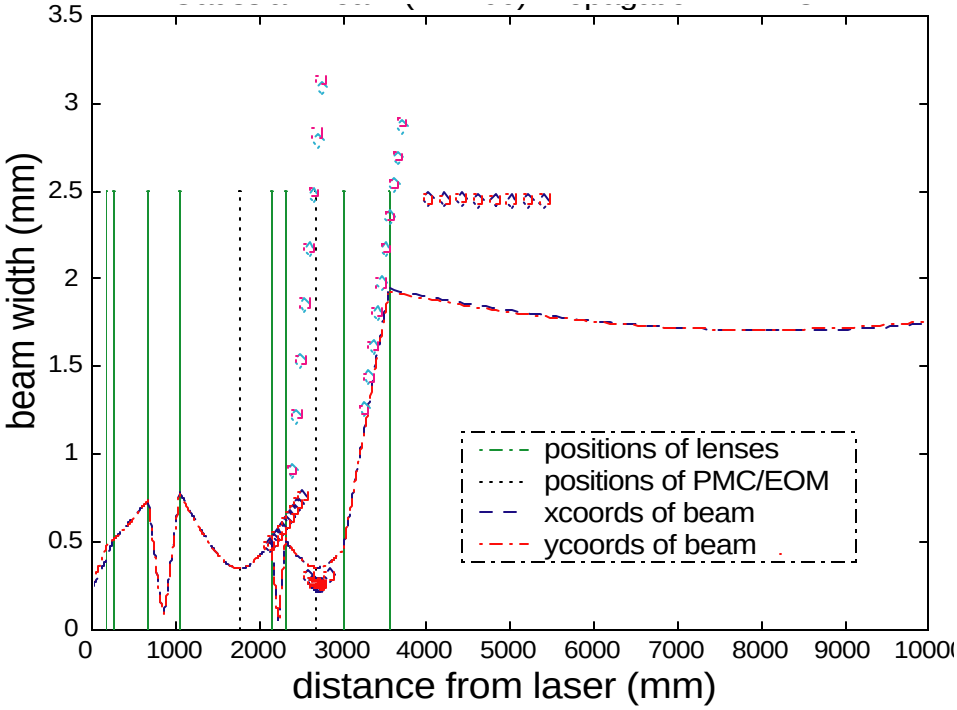

Figure 12: Beam Propagation. **The red and blue makers are data we took.**

Table 2: Waist size and waist position

	From PSL to L1(mm)	From L1 to L2(mm)	From L2 to L3(mm)	From L3 to L4(mm)
Waist size	0.34	0.055	0.35	0.12

According to the result shown in Figure 12, the original design and present condition show a good coincidence near the Pre-mode cleaner but there is a big difference between them at the other locations. Therefore, we should adjust the mode matching lenses to fit the present beam to original design.

4.2 Adjusting mode matching lenses

We use a Matlab-based calculation to estimate the error of the location of the mode matching lenses according to the measurements of the beam widths from the previous data, and adjust the lenses in the following way. The right side of the diagram defines the direction we change, whether plus and minus. Table 3 gives the distances along the beam path of the mode matching lenses, before and after adjustment.

L1.....+8m

L2.....+9m

L3.....+0.2m

L4.....+18m

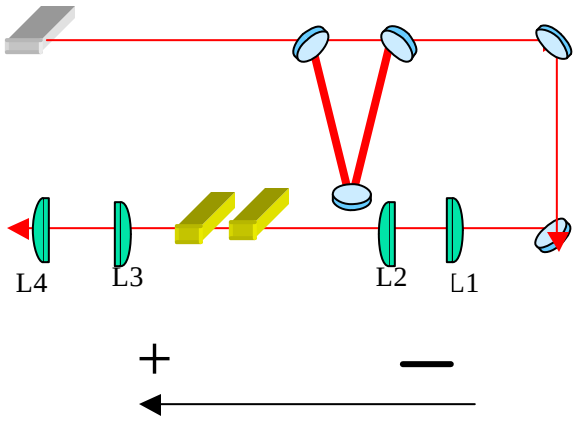

Table 3: Distance of mode matching lens before and after adjusting.

	PSLtoL1	L1 to L2	L2 to L3	L3 to L4	L4toMC
Before adjusting	377.0	1116.0	165.7	710	546.0
After adjusting	377.0	1099.0	165.5	692.0	546.0

4.3 Measurement of the beam profile after adjusting

After adjusting the lenses, the original design and the present beam are almost same, as shown in Figure 13.

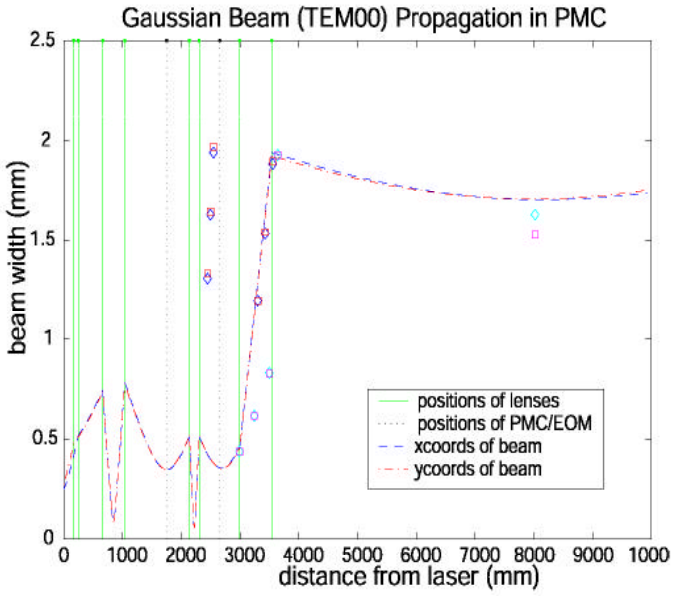

Figure 13: Beam width measurements after adjustment of mode matching lenses.

4.3.1 Amount of transmitted light

After adjusting the mode matching lenses, we measure the ratio of reflected light of mode cleaner, and assume $r^2 + t^2 = 1$. r is amplitude reflectivity of the mode cleaner, and t is the amplitude transmissivity. The result of this measurement is shown in Figure 14. The transmition through the mode cleaner improves from 60% to 87%.

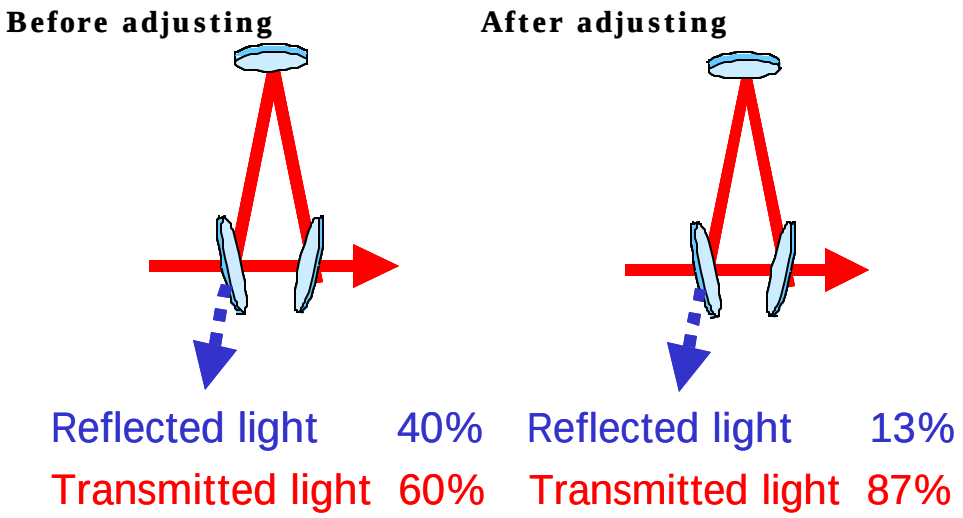

Figure 14: Improvement of transmitted light of mode cleaner

4.3.2 Mode Mismatch

The mode mismatch is defined by

$$MM = \left(\frac{w_{meas} - w_{design}}{w_{design}} \right)^2 + \left(\frac{z_{meas} - z_{design}}{2z_R} \right)^2 \quad (16)$$

W is the waist size, and Z is the position of waist. z_R is the Rayleigh length:

$$Z_R = \frac{pw_{design}^{\ 2}}{l} \quad (17)$$

Each of the parameters of equations (16) and (17) is shown in Table 4.

Table 4: Each of the parameters of the equation (16) and (17).

w_{meas} (mm)	1.7045
w_{design} (mm)	1.9296
$z_{meas} - z_{design}$ (m)	0.01
l (μm)	1.064

In this experiment, the mode mismatch is only 2.6%.

5 Position and Angle Sensors

In this experiment we install the angle and position sensors to monitor the fluctuation of the beam at the mode cleaner. For this purpose we use quadrant photodiodes (QPDs), and take the following three steps:

- Setup of the lenses for the angle and position sensors
- Calibration of the mode matching lenses.
- Monitoring for the fluctuation of the beam.

5.1 Set up of the position and angle sensors

While the main beam goes into the periscope, which is used to lift the beam to the height of the mode cleaner, some of the beam is picked off and goes into the Position and Angle sensing system.

We use QPDs to detect the information of each fluctuation in position and angle of the beam. QPDs have four photodetector surfaces, which give differential signals in the vertical and horizontal direction respectively. The power of ups and downs was balanced to measure the beam position, and the power of right and left was also as same as ups and downs. The beam size is controlled by setting the lenses before the beams go into the QPD, to an accuracy of about 2 mm. The Angle sensor is set on a far field not to detect the position but to detect the angle information. The Position sensor is the counterpart.

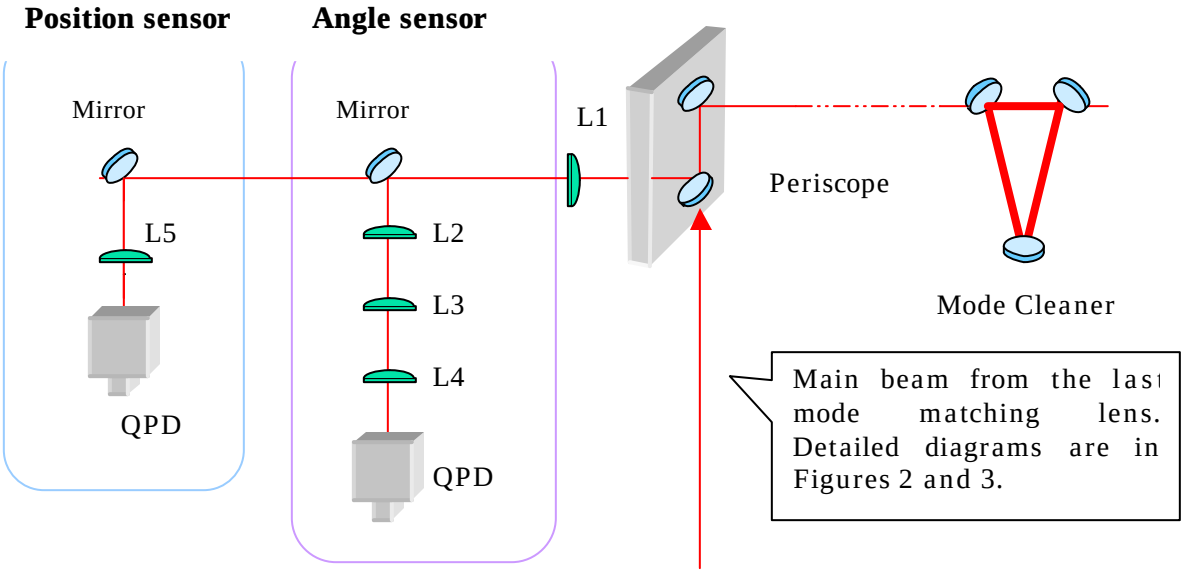

Figure 15: Set up of the position and angle sensors.

Table 5 lists the lenses for the setup the Position and Angle sensor. The first number in Table 5 is the curvature of the mirror, and second one is a diameter of the mirror.[4]

Table 5: Lenses used in front of the quadrant photodiodes in order to measure beam position and angle.

L1	L2	L3	L4	L5
PLCX-25.4-103-UV	PLCX-8.0-5.2-UV	PLCX-25.4-38.6-UV	PLCX-25.4-12.9-UV	PLCX-25.4-13.1-UV

5.2 Calibration

As the output of the QPD is described in units of the beam power (or more precisely, voltage), it is necessary to rewrite the information in units of displacement (m) or angle (radians), through a calibration procedure.

.

5.2.1 Set up experiments for the calibration

Since lenses can easily change the beam direction when the beam is miscentered, we decides to use a mirror for calibration, equipped with micrometers to shift the beam path, after the final lenses L4 and L5 (Fig.16).

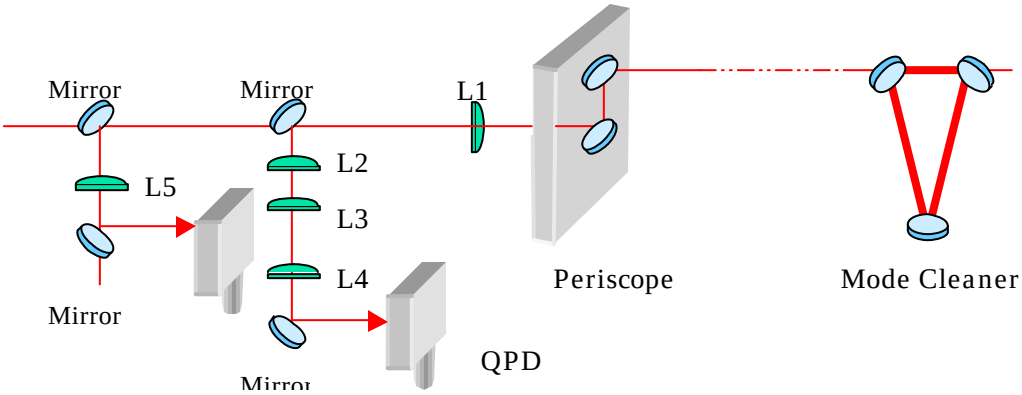

Figure 16: Set up for the calibration of the position and angle sensors.

5.2.2 Coefficient of the calibration

After setting up the lenses, we move the position and angle by a small, known amount, and record the QPD response in volts. In Figure 17, we can see there is a region in which the QPD's output is proportional to the displacement. The calibration coefficient is obtained as a proportion in this linear region.

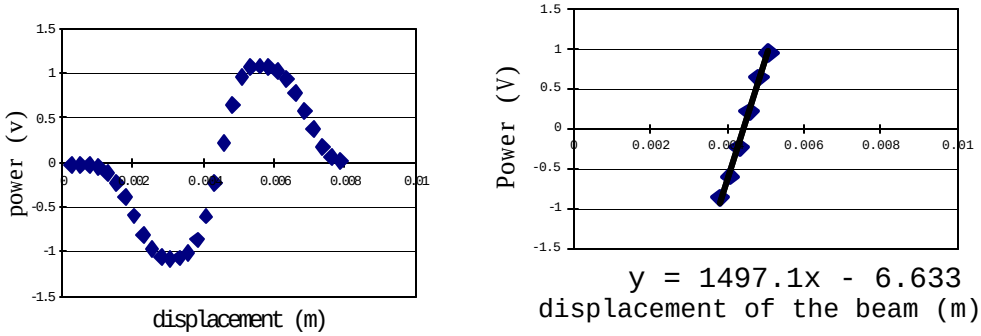

Figure 17: Calibration (V/m) of the position sensor. Left: over the full region. Right: in the central, linear region

For the position sensor, the coefficients for horizontal and vertical movement are 1.5 mV/mm and 1.3 mV/mm respectively. For the angle sensor, the coefficients are 1.1mV/mrad and 0.7 mV/mrad. Now we can change the voltage data to the displacement.

5.3 Results on the fluctuation of laser beam position and angle

We obtain the following results. Figure 18 shows the beam drift in position and angle over two days of monitoring. Figure 19 shows the spectra of the motion from 1 Hz to 1kHz.

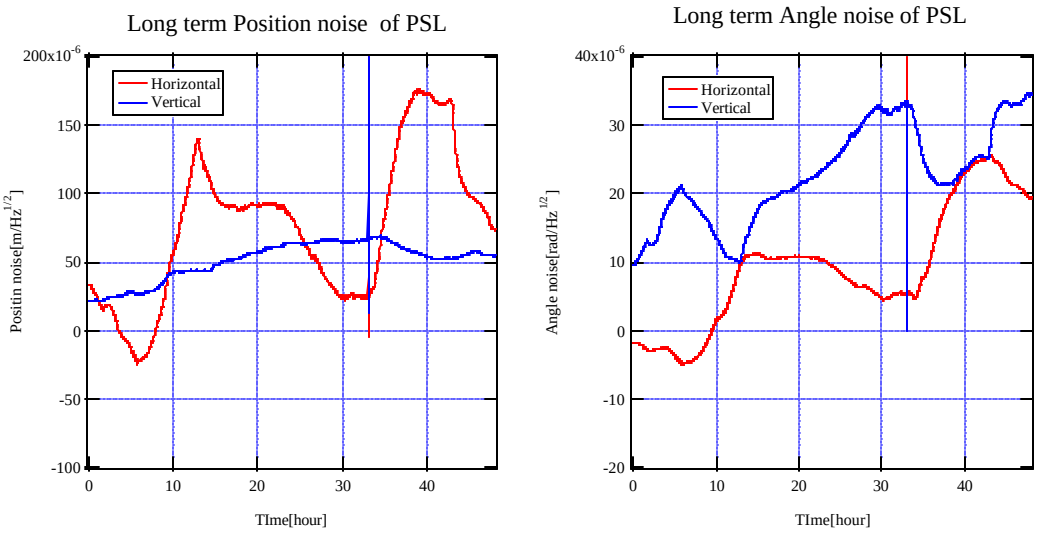

Figure 18: Long term position (left) and angle (right) drift of the PSL beam in the IOO monitoring system.

The saturated data at ~ 33 hours in both graphs of Figure 18 is caused by the Pre-mode Cleaner falling briefly out of resonance, and then, shortly thereafter, re-acquiring lock.

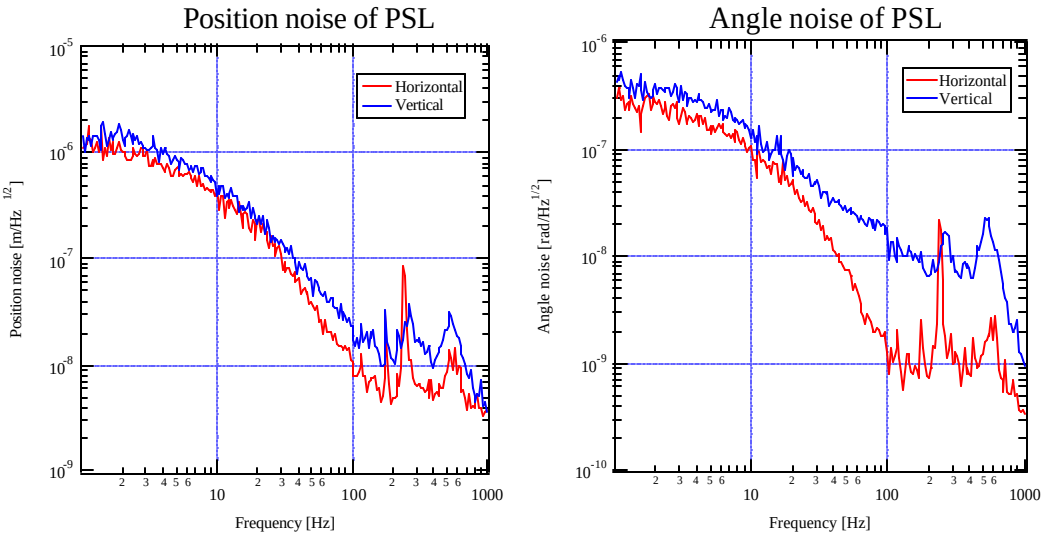

Figure 19: Position (left) and angle (right) noise amplitude spectrum of the PSL beam in the IOO monitoring system.

Both position and angle noise spectra fall with frequency until 100Hz. The noise has a peak around 200Hz, which is presumably due to some mechanical resonance on the PSL table.

6 Conclusions and Further Work

We have done two experiments. One is the mode matching for the mode cleaner, and the other one is the installation of the angle and position sensors to monitor the beam jitter at the point where the beam leaves the PSL table and is launched towards the mode cleaner.

In first experiment we adjusted the mode matching lenses until the observed transverse profile matched the design values. Consequently the transmitted light through the mode cleaner has been improved from 60% to 87%. We have succeeded in obtaining a circular Gaussian TEM00 mode profile by reducing the higher order gaussian modes, which had been observed quite a bit in the reflected light before the adjustment.

After this adjustment the mode cleaner achieved lock robustly. I believe that this is one of the benefits of our work, and I believe that our experiments have had a positive influence on the locking of the mode cleaner.

In the second experiment we installed the angle and position sensors to monitor the beam jitter at the mode cleaner. We have succeeded in monitoring the fluctuation. Further work is required to control this fluctuation by a feedback loop system using these monitoring data.

7 Acknowledgements

I would like to express my deepest gratitude to following people. Professor Alan Weinstein gives me grateful opportunities of working in 40m laboratory, and he always gave good advice for my experiment. Although he is quite busy, he correct my poor English and give me a lot of valuable comments when I wrote the Surf reports. And he always cheers me up. I am very happy to have been working under his teaches. The last day when I have to say good–by to him, I was so sad and I am almost crying. Osamu Miyakawa taught me how to experiment exactly. For first a few weeks I was not accustomed to use the laser. He showed me a good skills to use the laser. And almost all experiment introduced in this report are done under his teaches. And when I broke my personal computer, he also helped me to recover it. Michael Smith taught me the installation Angle and Position sensors. He looked for the needed lenses together, and ordered them. Kentarou Soumiya checked this report, and gave me good advice. And finally I want to express my thanks to Seiji Kawamura for encouraging me to join this Surf Project, and gave me this wonderful opportunity.

8 References

1. Peter R. Saulson, *Fundamentals of Interferometric Gravitational Wave Detectors* (World Scientific).
2. Anthony E. Siegman, *Lasers* (University Science Books Mill Valley, California).
3. Amnon Yariv, *Optical Electronics* (Harcourt Brace Jovanovich College Publishers).
4. Michael Smith, *IO Position and Angle Sensing System 40M IFO* (LIGOT020119-00-D).